Printed Circuit Board Coil Design with Reduced Series Resistance for High Power Inductive Wireless Power Transmission Systems

Alexis Narvaez A.
Dept. Electronic Engineering and Communications, I3A
Universidad de Zaragoza
Zaragoza, Spain
alexisna@unizar.es

Claudio Carretero
Dept. Applied Physics, I3A
Universidad de Zaragoza
Zaragoza, Spain
ccar@unizar.es

Jesus Acero
Dept. Electronic Engineering and Communications, I3A
Universidad de Zaragoza
Zaragoza, Spain
jacero@unizar.es

Jose M. Burdio
Dept. Electronic Engineering and Communications, I3A
Universidad de Zaragoza
Zaragoza, Spain
burdio@unizar.es

***Abstract*—Due to the growing use of the popular wireless power transmission (WPT) technology, an innovative method of coil design and optimization is presented in this paper. This method has been applied to develop spiral printed circuit board (PCB) coils with litz-wire structure. From the geometry definition, the design process is carried out by means of finite element analysis (FEA). In addition, as a complement to the design process, some prototypes of spiral PCB coils were built to contrast the simulation results and experimental measurements by means of the small-signal characterization, which reflects the success of the applied method.**

Keywords— IPT, WPT, inductive charging, PCB coils, wireless power transmission, induction system, home appliances

I. Introduction

The Wireless Power Transfer (WPT) technology has become very popular in the last decade because of the promising applications that are currently being implemented in the latest electronic systems. Among the most relevant applications of this technology at short-medium distances, the following can be mentioned: induction heating, [1], wireless power supply for medical implants, [2], and static or dynamic charging of electric vehicles, [3]. From a general perspective of technical challenges that battery-powered devices are facing, the wireless power transmission offers a new pattern of energization for electric-driven devices, which helps to reduce limitations of cost, heavy weight, low power density, etc., [4]. Some roadmaps to follow in the short-term are presented in [5].

The more usual and popular WPT technology at short-medium distances is the Inductive Power Transmission (IPT), Fig. 1, whose key elements are the transmitter and receiver coils, [6]. Because of the growing use and implementation of WPT technology in today's electronic systems, an innovative method of coil design and optimization is presented in this paper, that has been applied to develop large-size spiral printed circuit board (PCB) coils with litz-wire structure. Their use is steadily increasing because, starting from a single design, the manufacturing process can be fully automatic and a high level of homogeneity and repeatability can be obtained among the coils produced.

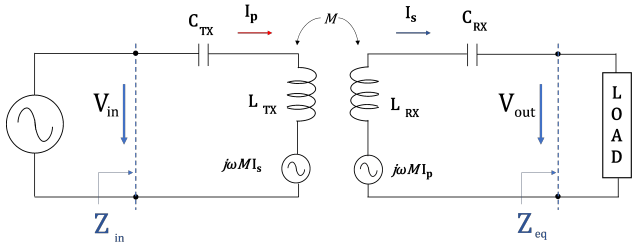

Fig. 1. Simplified inductive wireless power transmission system

Regarding related studies, in [7] a PCB coil design for IPT systems of medium voltage (MV) applications is presented with a single layer and multi stranded turns, it was achieved a global efficiency of 67% at 60 mm of air gap between coils, and in [8], analysis of partially split conductors in squared PCB coils shows clear evidence of decreasing series coil resistance. In [9] is widely analyzed the feasibility of printed PCB coils for electric vehicles (EV) wireless charging, the use of a four layer PCB coil in the receiver side offer good efficiencies compared to the conventional litz-wire coil, delivering around 3.3 kW.

In this work, the first step is to define the geometry of the coils, e.g. internal and external radii, number of turns and the approximate values of the electrical parameters to be obtained, then, the optimization design is based on the analysis and results of FEA models.

This paper is organized as follows. In section II the 2D - axisymmetric simulation model is introduced applied to spiral PCB coils. Section III presents the methodology of the design process in order to minimize the series resistance of the coils, which is directly reflected in the power losses of the windings, thus improving the global efficiency of the whole system. In Section IV, the experimental small-signal parameter characterization of the built prototypes and comparisons with simulation results are presented. Finally, in Section V several conclusions are drawn from the results obtained, and some

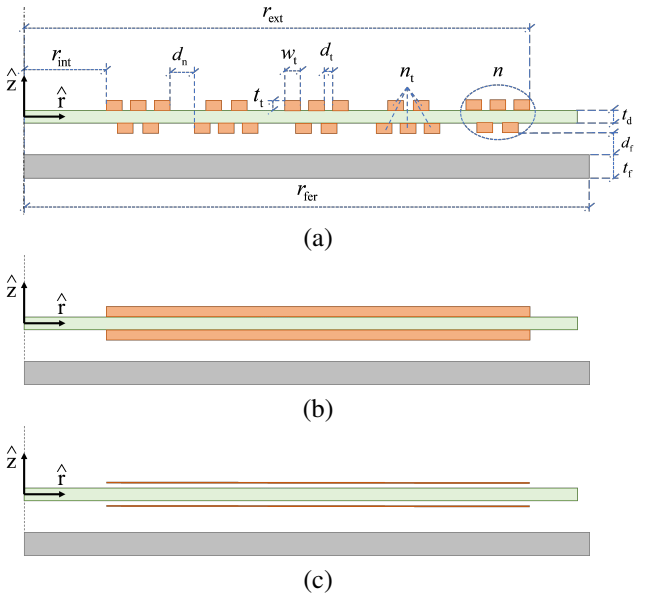

Fig. 2. 2D - axisymmetric FEA models varying in complexity: a) Multi-stranded turn, b) Double-block coil, c) Double-foil coil

short-term future lines are proposed.

II. Finite Element Model Description

This section presents the proposed FEA models whose results are used during the design process.

In order to speed up the optimization process with a low computational cost, 2D FEA models with rotational symmetry are proposed, as they are shown in the Fig. 2. The multi-stranded coil model, Fig. 2 (a), is the most detailed model and takes into account all the geometric characteristics of the coil. The double-block coil model, Fig. 2 (b), represents each copper layer as a conductor block but without internal structure. The double-foil coil model, Fig. 2 (c), represents each copper layer as a conductor foil without any internal structure. The notation used in this analysis is shown in the Fig. 2 (a) and TABLE I. This type of model has several advantages such as ease and speed of design, as well as low computational resource requirements. In our case study, it is highly recommended due to the axial symmetry of a coil.

A 3D model can be convenient when more accurate results are needed because they offer a better description of the core structure, but on the other hand, they are more expensive in terms of time and computational resources. They are also recommended when the system geometry does not have rotational symmetry, i.e. with non-circular windings or ferrite bars. However, these types of model are out of scope of this paper and will be part of future analyses.

A. Self-inductance calculation

In the frequency domain, the induced voltage, V_{coil} , is calculated by integrating the electric field, E_φ, along the length of the coil. When applying a external current density to the multi-stranded and double block coil models, Fig. 2 (a) and Fig. 2 (b), it is calculated, [10]:

TABLE I
Symbology used for FEA model parameters

External radius	r_{ext}	Track width	w_{t}
Internal radius	r_{int}	Track thickness	t_{t}
Number of turns	n	Dielectric thickness	t_{d}
Number of tracks	n_{t}	Ferrite distance	d_{f}
Distance between turns	d_{n}	Ferrite thickness	t_{f}
Distance between tracks	d_{t}	Ferrite radius	r_{fer}

$$V_{\text{coil}} = -\frac{1}{S_{\text{turn}}} \int_{S_{\text{coil}}} 2\pi r E_\varphi ds \tag{1}$$

where S_{coil} is the total cross-sectional area of the coil, and $S_{turn} = \frac{S_{coil}}{n}$ is the area of each turn.

On the other hand, when applying a surface current density to the double-foil coil model, Fig. 2 (c), the induced voltage:

$$V_{\text{coil}} = -\frac{1}{W_{\text{turn}}} \int_{w_{\text{coil}}} 2\pi r E_\varphi dl \tag{2}$$

where $w_{\text{coil}} = r_{\text{ext}} - r_{\text{int}}$ is the total width, and $W_{\text{turn}} = \frac{w_{\text{coil}}}{n}$ is the width of each turn, in the radial direction.

The equivalent impedance of the coil can be calculated by the ratio between the induced *emf* in the coil and the current carried by the coil, i.e., $Z_{\text{coil}} = \frac{V_{\text{coil}}}{I_{\text{coil}}}$. So that, the self-inductance of the spiral PCB coil can be obtained as:

$$L_{\text{coil}} = Im\left(\frac{Z_{\text{coil}}}{\omega}\right) \tag{3}$$

where the angular frequency is given by: $\omega = 2\pi f$, and f is the frequency in Hz of the current applied to the coil. The real part of (3) is null because an ideal coil has been modeled.

B. Series Resistance calculation

The series resistance of the coil is composed of the conduction and proximity resistances, [10]. The conduction resistance, R_{cond}, includes DC losses and losses associated with the skin effect, while the proximity resistance, R_{prox}, considers the power dissipated by the induced current in the inductors by a transverse and external varying magnetic field, [11].

The total resistance of a coil can be calculated as follows:

$$R_{\text{w}} = R_{\text{cond}} + R_{\text{prox}} \tag{4}$$

Due to the fact that in a PCB coil the conductors do not have symmetry in their cross-section area as round cables do, the following is the analysis performed to calculate the resistance components in rectangular cross-sectional conductors, [12].

1) Conduction resistance in rectangular cross-sectional conductors: For a PCB coil with a single conductor, the conduction resistance can be expressed as follows, [12]:

$$R_{\text{cond, u.l.}} = \frac{1}{w_{\text{t}}\, t_{\text{t}}\, \sigma}\, \Phi_{\text{cond}}\left(w_{\text{t}}, t_{\text{t}}, \delta\right) \tag{5}$$

where w_t and t_t are the width and thickness of the conductor respectively. The function Φ_{cond} includes the frequency dependence of proximity losses in rectangular conductors, and usually, it has a value around $\Phi_{cond} \sim 1$.

The mean length turn for a coil with n turns can be calculated as follows:

$$MLT = \sum_{i=1}^{n} [2\pi a_i] = n\, 2\pi \frac{(r_{int} + r_{ext})}{2} \tag{6}$$

where a_i is the radius of the i-turn.

Therefore, the total conduction resistance for a coil with n_t tracks can be obtained in the following way:

$$R_{cond} = \frac{MLT}{n_t w_t\, t_t\, \sigma}\, \Phi_{cond}\,(w_t, t_t, \delta) \tag{7}$$

2) Proximity resistance in rectangular cross-sectional conductors: To calculate the proximity resistance, it is convenient to use the orthogonal decomposition of the magnetic field strength applied to the conductors, [13]:

$$\mathbf{H}_0^2 = \mathbf{H}_{0,z}^2 + \mathbf{H}_{0,r}^2 \tag{8}$$

where $\mathbf{H}_{0,z}^2$ and $\mathbf{H}_{0,r}^2$ are the axial and radial component, respectively.

This suggests that the proximity losses in a conducting rectangle can be obtained by summing the losses generated by two parallel and orthogonal fields to its main directions:

$$\mathbf{P}_{prox}^2 = \mathbf{P}_{prox,\,z}^2 + \mathbf{P}_{prox,\,r}^2 \tag{9}$$

where $\mathbf{P}_{prox,\,r}^2$ and $\mathbf{P}_{prox,\,z}^2$ are the power losses induced by $\mathbf{H}_{0,r}^2$ and $\mathbf{H}_{0,z}^2$ respectively.

The proximity losses induced by each field component can be written as follows:

$$\mathbf{P}_{prox,\,u.l.,\,z} = \frac{2\pi}{\sigma}\, \Phi_{prox,\,z}\,(w_t, t_t, \delta)\, |\mathbf{H}_{0,z}|^2 \tag{10}$$

$$\mathbf{P}_{prox,\,u.l.,\,r} = \frac{2\pi}{\sigma}\, \Phi_{prox,\,r}\,(t_t, w_t, \delta)\, |\mathbf{H}_{0,r}|^2 \tag{11}$$

where $\Phi_{prox,\,z}$ and $\Phi_{prox,\,r}$ includes the dependence of proximity losses in rectangular cross-sectional area conductors due to the working frequency and their geometry, [13].

The losses associated with the series coil resistance due to the magnetic field generated by the current flowing through the coil, i.e. $\mathbf{H}_{0,z}^2$ and $\mathbf{H}_{0,r}^2$, are as follows, [10]:

$$\mathbf{P}_{prox,\,u.l.,\,z} = \frac{1}{2} R_{prox,\,u.l.,\,z} I_0^2 \tag{12}$$

$$\mathbf{P}_{prox,\,u.l.,\,r} = \frac{1}{2} R_{prox,\,u.l.,\,r} I_0^2 \tag{13}$$

And the proximity resistances per unit length of conductor are, respectively:

$$R_{prox,\,u.l.,\,z} = \frac{4\pi}{\sigma}\, \Phi_{prox,\,z}\,(w_t, t_t, \delta)\, \overline{\mathbf{H}}_{0,z}^2 \tag{14}$$

$$R_{prox,\,u.l.,\,r} = \frac{4\pi}{\sigma}\, \Phi_{prox,\,r}\,(t_t, w_t, \delta)\, \overline{\mathbf{H}}_{0,r}^2 \tag{15}$$

TABLE II
PARAMETERS VALUES ESTABLISHED FOR ANALYSIS

r_{ext} (mm)	190	t_t (μm)	70	140	210
r_{int} (mm)	90	d_n (μm)	250	375	500
n	8	d_t (μm)	250	375	500
t_d (mm)	1.55	t_f (mm)	5		
d_f (mm)	1	r_{fer} (mm)	201		

where $\overline{\mathbf{H}}_{0,z}^2$ and $\overline{\mathbf{H}}_{0,r}^2$ are the square of the external varying magnetic field generated by a current I_0, i.e., they represent the square of the normalized orthogonal fields.

As well as in the conduction losses, for a coil with several n turns and n_t tracks, the conduction resistance can be obtained as follows:

$$R_{prox,\,z} = n_t MLT \frac{4\pi}{\sigma}\, \Phi_{prox,\,z}\,(w_t, t_t, \delta)\, \overline{\mathbf{H}}_{0,z}^2 \tag{16}$$

$$R_{prox,\,r} = n_t MLT \frac{4\pi}{\sigma}\, \Phi_{prox,\,r}\,(t_t, w_t, \delta)\, \overline{\mathbf{H}}_{0,r}^2 \tag{17}$$

Finally, the total coil resistance for a spiral PCB coil with a rectangular cross-sectional area can be expressed as the sum of all the shown previous contributions:

$$R_w = R_{cond} + R_{prox,\,r} + R_{prox,\,z} \tag{18}$$

III. Optimization Methodology

In order to obtain coils with a high quality factor, the value of the series resistance of the coil should be reduced as much as possible. To design a spiral PCB coils with litz-wire structure, two methods complementary to each other are presented in this section. The first one takes into account the internal structure of the coil such as: the number of turns and tracks, the track width, the distance between tracks, the distance between turns, and the internal and external radii. The second one takes into account manufacturer restrictions, such as: the minimum diameter of a via to apply the transposition pattern to get a litz-wire structure, and the minimum width of the track that depends on the selected thickness copper.

A. Coil Geometry

To establish the geometrical parameters, a slight reference was taken from the SAE J2954 standard, which contains several guidelines when implementing wireless charging for electric vehicles. The chosen parameters are presented in the TABLE II for three different copper thicknesses. A coil in air and over a ferrite flux concentrator were analyzed to contrast the proposed models. The results of the magnetic field strength obtained at 85 kHz from the 2D double-foil coil model were used in this analysis, because it has no internal structure, in a way similar to a non-dimensional analysis.

First, the variation in self-inductance when changing the internal and external radii of the coils was analyzed. When $r_{ext} = 190$ mm and r_{int} varies, Fig. 3 (a), the obtained self-inductance value has more variability than the other case when r_{ext} varies and $r_{int} = 90$ mm, Fig. 3 (b). This variation must be

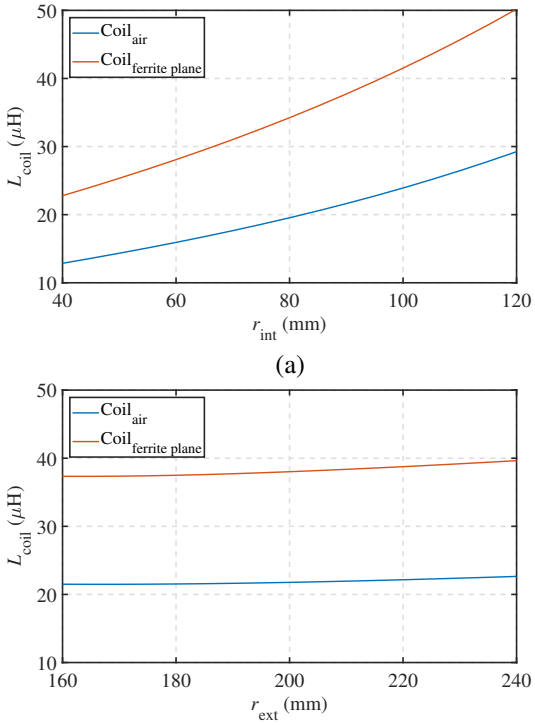

Fig. 3. Simulation results of the 2D double foil coil model with n = 8. Self-inductance variation: a) r_{ext} = 190 mm and r_{int} variable, b) r_{int} = 90 mm and r_{ext} variable

taken into account when it comes to the geometric definition if an specific value of self-inductance is required.

For the coils with the geometry of the TABLE II, the expected self-inductance values are around 21 μH and 37 μH for the coil in air and over ferrite, respectively. There is no noticeable role of the copper thickness in the variation of self-inductance due to the geometrical relationship between the distance occupied by the coil in the r-direction and the z-direction: $\frac{r_{ext}-r_{int}}{t_t}$. It can be also observed the change in the self-inductance due to the magnetic flux concentrator.

B. Geometric optimization

This analysis has taken into account the current limitations of the manufacturing process, in terms of track spacing and clearance, to set the specific parameters of the TABLE II.

According to the Fig. 2 (a), the following equations can be defined. The range of the width of each turn available in the radial direction can be calculated by subtracting the whole available radial distance minus the distance between turns:

$$\triangle\, r_{\mathrm{i}} = \frac{r_{\mathrm{ext}} - r_{\mathrm{int}} - d_{\mathrm{n}}\,(n-1)}{n} \tag{19}$$

The total number of tracks has to be divided into two layers, so there is necessary to split them in the way:

$$n_{\mathrm{t}} = n_{\mathrm{t,sup}} + n_{\mathrm{t,inf}} \Longleftrightarrow n_{\mathrm{t,sup}} = \frac{(n_{\mathrm{t}}+1)}{2}, n_{\mathrm{t,inf}} = \frac{(n_{\mathrm{t}}-1)}{2} \tag{20}$$

TABLE III
BEST RESULTS OF THE TOTAL RESISTANCE, GEOMETRIC OPTIMIZATION

Parameter	Coil in air			Coil over a flux concentrator		
n	8					
t_{t} (μm)	70	140	210	70	140	210
d_{n} (μm)	250	375	500	250	375	500
d_{t} (μm)						
n_{t}	23			31		27
w_{t} (μm)	794	670	546	533	409	397
f (kHz)	85					
R_{cond} (mΩ)	95.25	56.76	46.56	105.04	68.56	54.22
$R_{\mathrm{prox,r}}$ (mΩ)	0.03	0.23	0.63	0.13	0.83	2.33
$R_{\mathrm{prox,z}}$ (mΩ)	8.80	9.94	8.02	12.91	11.52	13.43
R_{w} (mΩ)	104.09	66.94	55.21	118.09	80.92	69.99

where $n_{\mathrm{t,\,sup}}$ and $n_{\mathrm{t,\,inf}}$ are defined as the number of tracks of one turn in the top layer and in the bottom layer respectively. As mentioned before, n_{t} is an odd number.

The width of each track can be calculated in the way:

$$w_{\mathrm{t}} = \frac{\triangle\, r_{\mathrm{i}} - d_{\mathrm{t}}\,(n_{\mathrm{t,\,sup}} - 1)}{n_{\mathrm{t,\,sup}}} \tag{21}$$

Then by applying (7), (16), (17) and (18) the total resistance of a coil with rectangular cross section is obtained.

The best cases obtained of total resistance, R_{w}, for a coil in air and over ferrite at 85 kHz are shown in the TABLE III. As expected, the thicker the copper the better the results. For a coil in air, the optimum number of tracks was obtained to be 23, resulting in a total resistance of 104 mΩ, 66 mΩ and 55 mΩ for copper thicknesses of 70 μm, 140 μm and 210 μm, respectively. On the other hand, with a flux concentrator, the optimum number of tracks was obtained to be 31 for copper thicknesses of 70 μm and 140 μm, resulting in a total resistance of 104 mΩ and 55 mΩ, respectively, and for copper thickness of 210 μm, the optimum number of tracks obtained is 27, resulting in a total series resistance of 69 mΩ.

The effect of including a flux concentrator can also be observed. The optimum number of tracks is higher due to the increase in the proximity resistance components, and to a greater extent the z-component.

C. Parametric optimization

In this subsection, a parametric sweep of the geometric parameters of each single track is presented. This analysis shows the value of the total resistance as a function of increasing width and thickness of a track, and the total number of tracks of the coil. To calculate the contour limits of the series resistance, the results of the model without internal structure double foil coil, Fig. 2 (c), have been used.

According to the Fig. 2 (a), the equation is defined:

$$w_{\mathrm{t,\,end}} = \frac{\triangle\, r_{\mathrm{i}}}{n_{\mathrm{t,\,sup}}} \tag{22}$$

where $w_{\mathrm{t,\,end}}$ is the width of a track that includes the distance between tracks, i.e., $w_{\mathrm{t}} + d_{\mathrm{t}}$.

The minimum distance between tracks can be defined as:

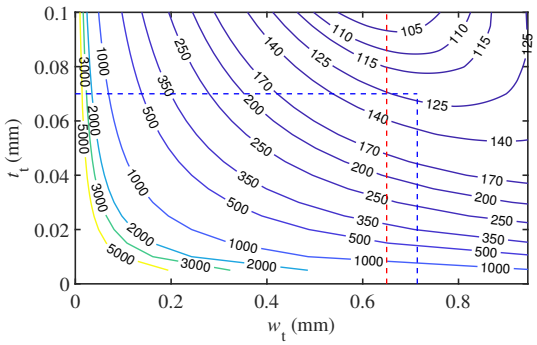

Fig. 4. Total resistance of the coil over ferrite , R_w (mΩ), at 85 kHz with $n_t = 25$. Red limit: $w_{t,\,min} = 650$ μm, blue limit: $w_{t,\,max} = 713$ μm and $t_t = 70$ μm, $d_t = d_n = 250$ μm

TABLE IV
BEST RESULTS OF THE TOTAL RESISTANCE, PARAMETRIC OPTIMIZATION

Parameter	Coil in air			Coil over a flux concentrator		
n	8					
$w_{t,\,min}$ (μm)	650					
t_t (μm)	70	140	210	70	140	210
d_n (μm)	250	375	500	250	375	500
d_t (μm)						
n_t	23		19	25	23	19
$w_{t,\,max}$ (μm)	794	670	756	713	670	756
f (kHz)	85					
R_w (mΩ)	104.25	67.89	57.45	125.25	91.01	86.11

$$d_{t,\,min} = (w_{t,\,end} - w_{t,\,max})\,\frac{n_{t,\,sup}}{n_{t,\,sup} - 1} \tag{23}$$

where $w_{t,\,max}$ is the maximum width of a track taking into account the minimum distance between tracks, i.e. $w_t + d_{t,\,min}$. The value of d_t in the TABLE II was set as the minimum allowable distance between tracks.

To calculate $w_{t,\,max}$ it is necessary to isolate it in the way:

$$w_{t,\,max} = w_{t,\,end} - d_{t,\,min}\,\frac{n_{t,\,sup} - 1}{n_{t,\,sup}} \tag{24}$$

To take into account technology constraints, a minimum drilling diameter has been set to Ø $\text{drill}_{min} = 250$ μm, and the minimum copper ring diameter to Ø $\text{ring}_{min} = 650$ μm. From this, to maintain the width of the copper ring along all the tracks, the minimum track width has also been set to $w_{t,\,min} = 650$ μm.

According to the TABLE III, for copper thicknesses $t_t = 70$ μm and 140 μm the geometrical optimal number of tracks is $n_t = 31$, and for $t_t = 210$ μm is $n_t = 27$. Although the calculated number of tracks are the optimum in each case, the restriction $w_{t,\,min}$ is not satisfied. To met all geometric and manufacturing restrictions, a feasible number of tracks, based on copper thicknesses of $t_t = 70$ μm, 140 μm and 210 μm was calculated to be $n_t = 25$, 23 and 19, respectively.

The obtained result for the copper thickness $t_t = 70$ μm is presented as contour limits of the total resistance value, R_w, Fig. 4. The plotted red limit is the minimum track width to met restriction $w_{t,\,min} = 650$ μm. The TABLE IV shows a brief summary of the results in each case.

This analysis offers a global view of the design parameters of major impact that can be adjusted according to a criterion of the possible minimum local value obtained, but on the other hand, each number of tracks has an specific parametric sweep.

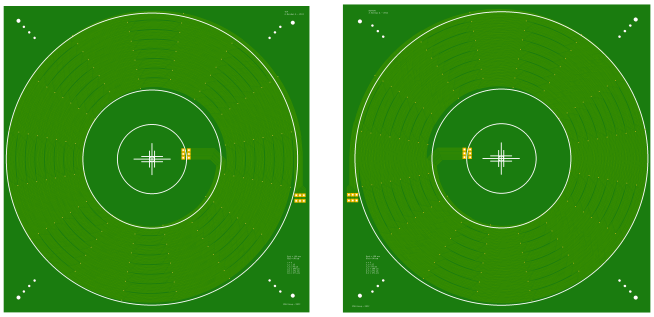

(a) (b)

Fig. 5. Spiral PCB Coil designed, $t_t = 70$ μm , $n_t = 25$, a) Top, b) Bottom

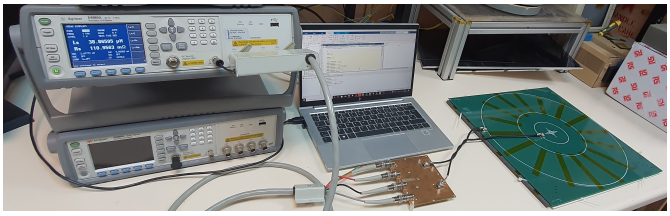

Fig. 6. Experimental set-up of the characterization. Coil over a ferrite flux concentrator.

IV. Experimental Validation

The Fig. 5 shows the prototype PCB coil with litz-wire structure built with the assistance of the automated design PCB generator presented in [14], as it only needs the specific geometrical parameters to generate it. The methodology applied is validated by characterizing the prototype with a high-precision LCR meter and the experimental set-up is shown in the Fig. 6. it is necessary to

The contrast of experimental and simulation results of the series resistance and self-inductance are depicted in the Fig. 7. A good fit between experimental measurements and simulation results can be observed, but at frequencies above 400 kHz capacitance parasitic effects are noticeable in the experimental measurements because the proposed FEA models do not take into account parasitic elements, i. e., an ideal coil is modeled.

V. Conclusions

There can be extracted several interesting conclusions from the analysis presented before.

After establish the general geometric features of the coil, an odd number of tracks must be selected to apply the transposition pattern to get a litz-wire structure. While the geometric optimization can give to the designer a general overview of the optimum number of tracks to be chosen, the parametric optimization shows the variation of the coil

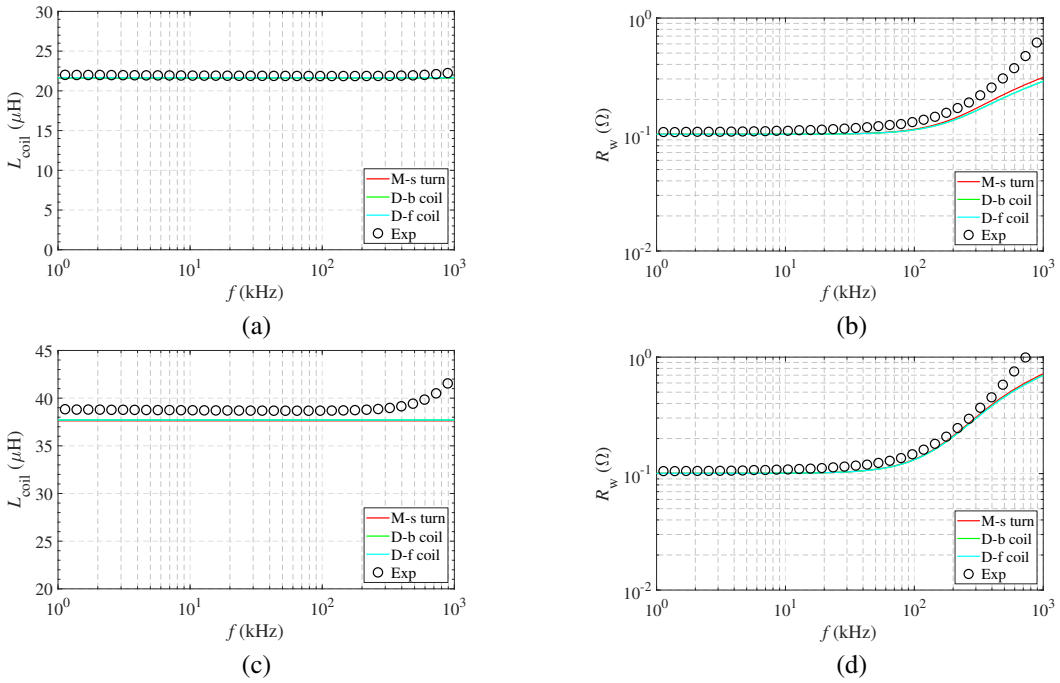

Fig. 7. Prototype coil characterization in the frequency domain, $n_t = 25$, $t_t = 70$ μm. Coil in air: a) L_{coil} , b) R_w. Coil over ferrite: c) L_{coil} , d) R_w

resistance taking into account manufacturing restrictions. The proposed ideal FEA models show accurate results, although capacitance parasitic effects can be observed in the experimental measurements at frequencies above 400 kHz. However, these parasitic effects are noticeable at frequencies much higher than the operation of the developed system. By means of small-signal characterization of a prototype coil the design methodology was validated because of the good fit in the contrast performed.

Finally, it is proposed to build 3D coil models for comparison with the 2D models, and apply the methodology described in this work. Coil performance tests under real working conditions are necessary to determine the suitability of the spiral PCB coils for high power IPT systems.

ACKNOWLEGMENT

This work was partly supported by the Spanish MICINN and AEI under Project PID2019-103939RB-I00 and Project PDC2021-120898-I00, co-funded by EU through FEDER and NextGenerationEU/PRTR programs, by the DGA-FSE, and by the BSH Home Appliances Group.

REFERENCES

[1] O. Lucia, J. Acero, C. Carretero, and J. Burdio, "Induction Heating Appliances," *IEEE Industrial Electronics Magazine*, vol. 1, no. September, pp. 35–47, 2013.

[2] O. Knecht and J. W. Kolar, "Performance Evaluation of Series-Compensated IPT Systems for Transcutaneous Energy Transfer," *IEEE Transactions on Power Electronics*, vol. 34, no. 1, pp. 438–451, 2018.

[3] A. Ahmad, M. S. Alam, and R. Chabaan, "A Comprehensive Review of Wireless Charging Technologies for Electric Vehicles," *IEEE Transactions on Transportation Electrification*, vol. 4, no. 1, pp. 38–63, 2017.

[4] Z. Zhang, H. Pang, A. Georgiadis, and C. Cecati, "Wireless Power Transfer - An Overview," *IEEE Transactions on Industrial Electronics*, vol. 66, no. 2, pp. 1044–1058, 2019.

[5] H. T. Nguyen, J. Y. Alsawalhi, K. A. Hosani, A. S. Al-Sumaiti, K. A. A. Jaafari, Y. J. Byon, and M. S. E. Moursi, "Review Map of Comparative Designs for Wireless High-Power Transfer Systems in EV Applications: Maximum Efficiency, ZPA, and CC/CV Modes at Fixed Resonance Frequency Independent from Coupling Coefficient," *IEEE Transactions on Power Electronics*, vol. 37, no. 4, pp. 4857–4876, 2022.

[6] A. A. Narvaez, C. Carretero, J. Acero, and J. M. Burdio, "An Inductive Power Transfer System Case Study: Large Gap in Low Power Wireless Power Supply," *IEEE International Symposium on Industrial Electronics*, vol. 2020-June, pp. 649–654, 2020.

[7] X. Du, C. Li, and D. Dujic, "Design and Characterization of PCB Spiral Coils for Inductive Power Transfer in Medium-Voltage Applications," *IEEE Transactions on Power Electronics*, vol. 37, no. 5, pp. 6168–6180, 2022.

[8] Y. Shin, J. Park, H. Kim, B. Park, J. Kim, C. Park, and S. Ahn, "A Wireless Charging Coil in Printed Circuit Board with Partially Split Conductors for Low Resistance," *2019 IEEE Wireless Power Transfer Conference, WPTC 2019*, pp. 366–370, 2019.

[9] A. Ramezani and M. Narimani, "An Efficient PCB Based Magnetic Coupler Design for Electric Vehicle Wireless Charging," *IEEE Open Journal of Vehicular Technology*, vol. 2, no. October, pp. 389–402, 2021.

[10] C. Carretero, "Coupling Power Losses in Inductive Power Transfer Systems With Litz-Wire Coils," *IEEE Transactions on Industrial Electronics*, vol. 64, no. 6, pp. 4474–4482, 2017.

[11] M. Lu and K. D. Ngo, "Analytical Calculation of Proximity-Effect Resistance for Planar Coil with Litz Wire and Ferrite Plate in Inductive Power Transfer," *IEEE Transactions on Industry Applications*, vol. 55, no. 3, pp. 2984–2991, 2019.

[12] I. Lope, J. Acero, J. M. Burdio, C. Carretero, and R. Alonso, "Design and implementation of PCB inductors with litz-wire structure for conventional-size large-signal domestic induction heating applications," *IEEE Transactions on Industry Applications*, vol. 51, no. 3, pp. 2434–2442, 2015.

[13] I. Lope, C. Carretero, J. Acero, R. Alonso, and J. M. Burdio, "Frequency-dependent resistance of planar coils in printed circuit board with litz structure," *IEEE Transactions on Magnetics*, vol. 50, no. 12, pp. 1–9, 2014.

[14] J. Serrano, I. Lope, J. Acero, C. Carretero, and J. M. Burdio, "Mathematical description of PCB-adapted litz wire geometry for automated layout generation of WPT coils," *Proceedings IECON 2017 - 43rd Annual Conference of the IEEE Industrial Electronics Society*, vol. 2017-Janua, no. 1, pp. 6955–6960, 2017.